Chemical Engineering Journal 435 (2022) 134924

Contents lists available at ScienceDirect

Chemical Engineering Journal

journal homepage: www.elsevier.com/locate/cej

TADF dendronized polymer with vibrationally enhanced direct spin-flip between charge-transfer states for efficient non-doped solution-processed OLEDs

Chensen Li [a,b], Alastair K. Harrison [c], Yuchao Liu [a,d], Zhennan Zhao [a], Fernando B. Dias [c], Cheng Zeng [d], Shouke Yan [a,d], Martin R. Bryce [b,*], Zhongjie Ren [a,*]

[a] State Key Laboratory of Chemical Resource Engineering, Beijing University of Chemical Technology, Beijing 100029, China
[b] Chemistry Department, Durham University, South Road, Durham DH1 3LE, UK
[c] Physics Department, Durham University, South Road, Durham DH1 3LE, UK
[d] Key Laboratory of Rubber-Plastics, Ministry of Education, Qingdao University of Science & Technology, Qingdao 266042, China

ARTICLE INFO

Keywords:
Dendronized polymer
Thermally activated delayed fluorescence
Aggregation-enhanced emission
Reverse intersystem crossing
Organic light-emitting diodes

ABSTRACT

A novel type of thermally activated delayed fluorescence (TADF) dendronized polymer was designed and synthesized. Firstly, one side of the asymmetric TADF unit was encapsulated by 3,6-di-*tert*-butylcarbazole via a conjugated linkage with strong twisted intramolecular charge transfer (TICT) to minimize the energy gap between ^{1}CT and ^{3}CT, and then the peripheral dicarbazole connects in a non-conjugated way on the other side, showing weak TICT and high-lying ^{3}LE&^{3}CT state; finally, a linear dendronized polymer, **PDCDC**, was obtained by introducing the alkyl polymer backbone as main chains. As far as we know, this is the first blue or greenish-blue-emitting TADF dendronized polymer. For **PDCDC**, the spin-forbidden ^{1}CT ↔ ^{3}CT transitions are activated by molecular vibrations, which combine with a small energy gap and reorganization energy to enable ^{1}CT ↔ ^{3}CT spin-flip transition rates reaching 10^6 s^{-1} with negligible role of a second triplet state. Films of **PDCDC** show a double exponential decay (prompt fluorescence and delayed fluorescence) in the presence of oxygen due to a low oxygen permeability ascribed to the entangled polymeric backbone which increases film density. Besides, obvious aggregation-enhanced emission (AEE) property can minimize the exciton quenching in aggregated states. A maximum external quantum efficiency of 9.0% for non-doped **PDCDC**-based organic light-emitting diodes (OLEDs) can be obtained. To the best of our knowledge, these are the most efficient dendronized polymer devices with blue or greenish-blue emission.

1. Introduction

E-type delayed fluorescence [1], which has been re-named thermally activated delayed fluorescence [2] (TADF) is an important mechanism for the efficient harvesting of the "dark" triplet states in organic molecules for light emission [3–5]. TADF requires the conversion of triplet excited states (T_1) into singlet states (S_1) through a reverse intersystem crossing (RISC) mechanism. A fast RISC rate is required to out-compete the non-radiative decay rate [6], and thereby a high photoluminescence yield can be obtained, including both prompt and delayed fluorescence. It is generally acknowledged that the prerequisites of an efficient TADF molecule is a narrow singlet–triplet energy gap (ΔE_{ST}), promoted by a small overlap between the highest occupied molecular orbital (HOMO) and the lowest unoccupied molecular orbital (LUMO) in molecules with strong intramolecular charge transfer (ICT), which can facilitate the energetically endothermic spin-flip process from T_1 to S_1 states [7]. However, in some cases, the simple two-electron two-state model fails to describe the real activation energy for RISC from the triplet state (^{3}CT) to the singlet state (^{1}CT) [8,9]. Previous investigations on CT states show that the spin–orbit coupling (SOC) between the ^{1}CT and ^{3}CT states is forbidden with $\langle {}^1CT|\hat{H}_{SOC}|{}^3CT\rangle \approx 0$ based on El-Sayed's rule [10], but hyperfine coupling (HFC) may be activated to facilitate the RISC when their energy gap is tiny (≤1 meV) [11]. However, the resulting RISC rate is still orders of magnitude too small to account for some experimental RISC rates. Therefore, a second-order spin-vibronic coupling mechanism based on a three-state model was proposed: an energetically-close or

* Corresponding authors.
E-mail addresses: m.r.bryce@durham.ac.uk (M.R. Bryce), renzj@mail.buct.edu.cn (Z. Ren).

https://doi.org/10.1016/j.cej.2022.134924
Received 2 December 2021; Received in revised form 14 January 2022; Accepted 24 January 2022
Available online 29 January 2022

degenerate intermediate triplet local excited state (^{3}LE) with nonadiabatic vibrational coupling plays an important role in mediating the spin-flip from ^{3}CT to ^{1}CT[12]. However, further investigations reveal that the energetic closeness of ^{3}LE does not reduce the activation energy of RISC but undesirably decreases the S_1-S_0 transition rate [13]. In terms of Marcus semiclassical electron-transfer theory [14], substantial differences in geometries and dipole moments of ^{1}CT and ^{3}LE states lead to large internal and external reorganization energies for the ^{1}CT↔^{3}LE transitions, which does not favor an efficient RISC process. Alternately, similar molecular vibrations and electronic structures between ^{1}CT and ^{3}CT states could minimize the reorganization energy, which is very important for achieving high rates of ISC and RISC [15]. Besides, it is well known that molecular vibrations are responsible for the violation of symmetry-forbidden and n-π* transitions rules [16]. Similarly, the transitions forbidden by the El-Sayed rule, based on the electronic nature of states, can be activated due to vibrational coupling perturbations. Accordingly, a vibrationally enhanced SOC model can describe the photophysics of TADF emitters when the energy gap and reorganization energy of ^{3}CT↔^{1}CT are very close [17]. Therefore, the design guideline of TADF polymer entails narrowing the lowest ^{1}CT and ^{3}CT gap while simultaneously elevating ^{3}LE above ^{3}CT state. The deep understanding of photophysical mechanisms is very helpful to develop efficient TADF materials for applications of organic light-emitting diodes (OLEDs) [18,19].

Traditional emitting materials of OLEDs are deposited by vacuum thermal evaporation, which may necessitate complicated technological processes, unavoidable material waste, and thus relatively high production costs. Solution processing techniques, such as spin-coating, spray-on and ink-jet printing, offer the advantages of rapid deposition at room temperature over large areas including flexible substrates [20], and they are drawing increasing attention due to their potential applications in low-cost, large-area and solid-state lighting. Owing to the beneficial combination of good solubility and high morphological stability, polymers are very suitable for solution-processed OLEDs [21]. In general, TADF polymers can be divided into conjugated and non-conjugated polymers [22]. Although, many conjugated TADF polymers have achieved impressive performance in polymer light-emitting diodes (PLEDs) [23], the inevitable red-shift of emission caused by conjugation makes it difficult to obtain efficient blue, or even blue-green emission [24]. In general, compared with the conjugated polymers, the non-conjugated side-chain-type TADF polymers are more likely to obtain blue emission by inheriting the characteristics of the TADF units in the side-chain. In general, non-doped TADF polymers are usually constituted by a non-conjugated backbone with pendant TADF units [25–28]. The connecting strategy can be divided into three types: (i) our group used a directly connected single bond to link the two components [25]; (ii) Yang's group adopted long alkyl chains as a linkage [26]; (iii) through-space charge-transfer between donors and acceptors is also being exploited by Wang's group [27,28]. However, these polymers are commonly synthesized by copolymerization of different monomer components, inevitably leading to random copolymerization, uncertainty of polymeric structures and intra/interchain energy transfers, and variable batch quality for characterization and device fabrication. In combination these factors may limit their device stabilities and practicalities [29]. Up to now, owing to the severe concentration quenching, homopolymers suffer from low electroluminescence efficiency of their devices [30].

Dendrimers with precise chemical structures allow perfect synthetic reproducibility, and their optoelectronic properties can be finely tuned through chemical decoration. They also show excellent stability, and solution processability; moreover, larger dendritic architectures prevent aggregation and reduce concentration quenching, which make them promising emitters material for OLEDs [31,32]. Therefore, some research groups [33–41] combined the effective control of interchromophore interactions of dendrimers with the desirable viscosity of polymers, and developed a series of poly(dendrimers) or dendronized polymers [33–35] that have a non-conjugated polymer backbone with dendrimer side-chains. The EQE of host-free green and red emissive poly (dendrimers) devices based on an iridium(III) complex can reach 11.7% (at 100 cd/m^2) [39] and 4.6% [40], respectively. However, efficient blue-emitting dendronized polymers and their devices (CIEy < 0.4) [42] are rarely reported up to now. The main limiting factor is that the construction of highly emissive emitters is hampered by the aggregation-caused quenching (ACQ) effect. For instance, traditional luminophores with planar and strong intermolecular interactions generally show bright emission in the mono-dispersed state, but weakened or even quenched emission in the aggregated state. Whereas, aggregation induced emission (AIE) and aggregation-enhanced emission (AEE) materials could avoid the undesirable ACQ effect and emit strongly in the aggregated state. In the mono-dispersed state, the active intramolecular motion boosts the non-radiative decay channels to quench emission, while in the aggregated state, the non-radiative decay channels are blocked due to the restriction of intramolecular motion, leading to enhanced emission [43–45]. Therefore, this is one class of the most promising materials to fabricate high-performance dendronized polymer OLEDs.

In this work, a new TADF dendronized polymer has been designed and synthesized; the structure is shown in Fig. 1. The linear dendronized homopolymer **PDCDC** has been obtained based on an asymmetric TADF unit, 10-(4-((4-(*9H*-carbazole-9-yl)phenyl)sulfonyl)-phenyl)-9,9-dimethyl-9,10-dihydroacridine (**DMAC-DPS-Cz**),[46] with a conjugated carbazole dendritic sub-structure and a non-conjugated branched tricarbazole unit. A non-conjugated alkane backbone was chosen to ensure a high triplet energy (E_T) of the main chain, whereas a conjugated backbone would have a lower E_T and potentially lead to unwanted triplet energy transfer from the TADF units to the backbone. The theoretical simulations found that the ^{1}CT ↔ ^{3}CT transitions are effectively activated by molecular vibrations due to the reduction of the ^{1}CT-^{3}CT energy gap and reorganization energy. In addition, AEE strategies were integrated into the emitter, which can effectively overcome the drawbacks of concentration quenching and achieve efficient solid-state luminescence. **PDCDC** has a small ΔE_{ST}, a short delayed fluorescence lifetime and excellent TADF performance. The non-doped solution-processable devices showed an EQE_{max} of 9.0%, which is the highest reported value based on blue and greenish-blue dendronized polymers. Non-doped devices have the merits of process simplicity and generally enhanced stability compared to conventional doped OLEDs [19].

2. Results and discussion

2.1. Synthesis and characterization

The multi-step syntheses of **PDCDC** are described in the Supporting Information (**Schemes S1-S2**). **PDCDC** was obtained by free radical polymerization of the corresponding vinyl-substituted monomer. The structures of the target material, and of the synthetic intermediates, were established by ^{1}H and ^{13}C NMR spectroscopy, mass spectrometry and elemental analysis (**Figure S1-S3**). The molecular weight (M_n) of **PDCDC** was 12.7 kDa and the polydispersity index (PDI) was 1.16 by gel permeation chromatography (GPC) (**Figure S4**). The target material has good solubility in common organic solvents such as chloroform, toluene, dichloromethane, chlorobenzene and tetrahydrofuran. **PDCDC** has a thermal decomposition temperature (T_d) with 5% weight loss range of 441 °C by thermal gravimetric analysis (TGA), and a glass transition temperature (T_g) of 93 °C, indicating moderate thermal stability (**Figure S5**).

2.2. Theoretical simulation

The molecular simulation of **PDCDC** by density functional theory (DFT) B3LYP/6-31G(d) by Gaussian 09 (Fig. 2**a**) shows the minimum energy molecular conformation and HOMO and LUMO distributions. As would be expected, the conjugation of the 3,6-di-*tert*-butylcarbazole

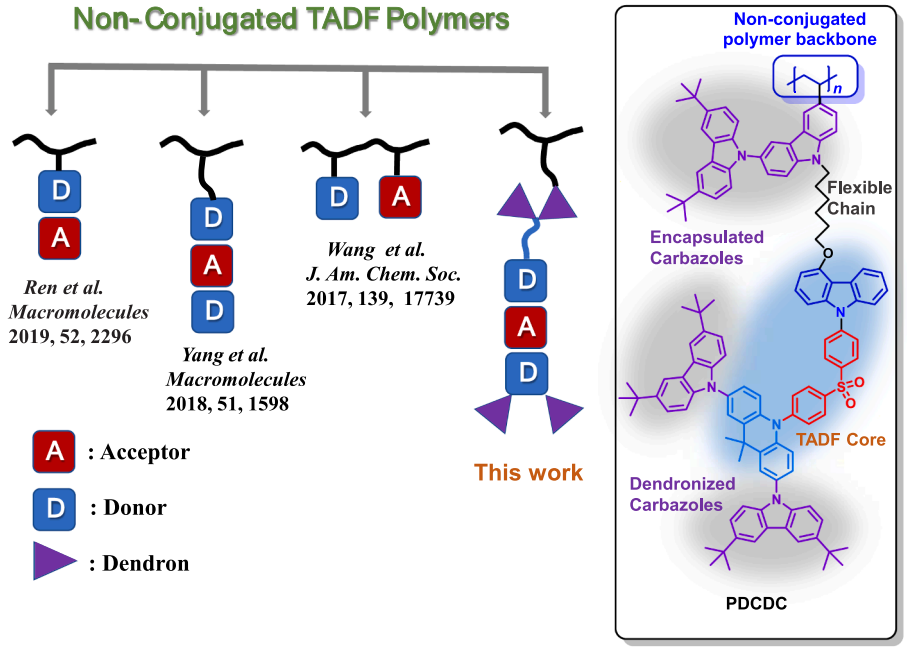

Fig. 1. Design strategies and structure for TADF polymers and the TADF polymer **PDCDC** for non-doped solution processable OLEDs.

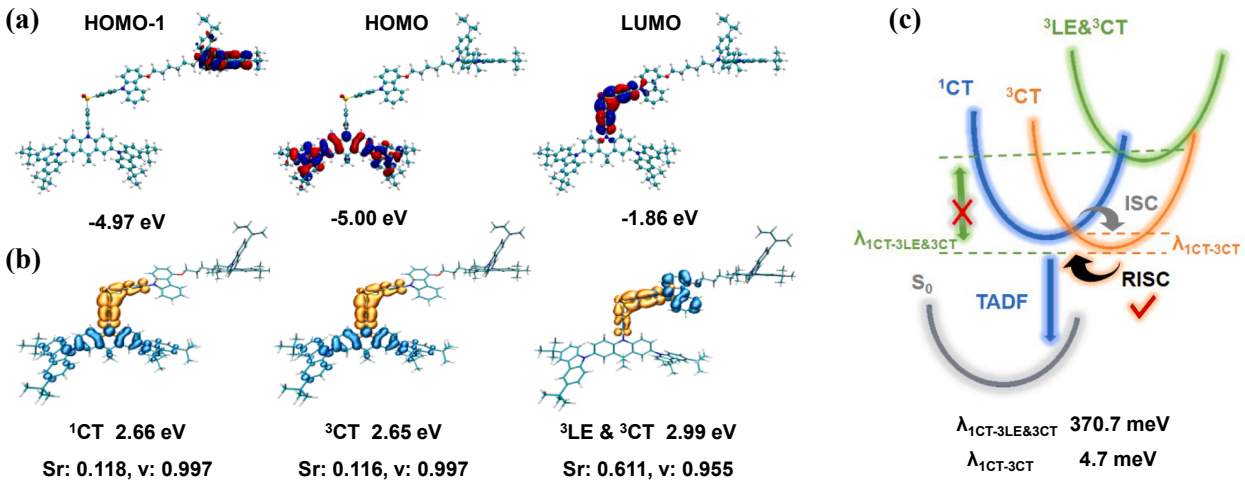

Fig. 2. Frontier orbital distributions (a), NTO analysis (b) and schematic diagram for plausible mechanism (c) of **PDCDC**. The abbreviations: ^{1}CT: singlet charge-transfer state, ^{3}CT: triplet charge-transfer state, ^{3}LE: triplet local state, Sr: the overlap integral of the hole-electron wave function, v: the weight of the hole-electron wave function's contribution to the excitation, RISC: reverse intersystem crossing, ISC: intersystem crossing, $\lambda_{1CT-3CT}$: reorganization energy between ^{1}CT and ^{3}CT, $\lambda_{1CT-3LE\&3CT}$: reorganization energy between ^{1}CT and ^{3}LE&^{3}CT.

units with acridan enhances the electron donating ability, and therefore HOMO distribution is mainly on these three subunits, while LUMO is mainly distributed on the diphenylsulfone (DPS) acceptor. This effective separation of HOMO and LUMO reduces ΔE_{ST} significantly, so **PDCDC** exhibits obvious TADF characteristics. Besides, the energy level of HOMO-1 is close to that of HOMO, but the electron distribution is localized in the isolated dicarbazole, indicating a good hole-transporting ability of the polymer. To discern more details about the excited state and their corresponding nature, TD-DFT analyses by Gaussian 09 were obtained to understand the excitation energy by using B3LYP/6-31G (d) method. The natural transition orbital (NTO) analyses (Fig. 2**b**) were performed to examine the nature of the excited states by Multiwfn [47]. Notable conformational features of **PDCDC** are: (i) a dihedral angle of 91° between the acridan donor and the attached phenyl ring of the DPS acceptor, indicating a strong TICT between acridan and DPS to achieve a low energy level of ^{1}CT and ^{3}CT with a small gap between them; (ii) a dihedral angle of 105° between the planes of the two phenyl rings of the DPS unit, which could ensure an obvious n-π* transition to shorten the valid conjugation length for upraised ^{3}LE; (iii) a dihedral angle of 49° between the plane of the carbazole donor and the plane of the attached phenyl ring of DPS acceptor and the relatively small dihedral angle could achieve a weak TICT with a high-lying second ^{3}CT hybrid with ^{3}LE state.

In addition, the hole and electron wave functions of the lowest ^{1}CT and ^{3}CT states of **PDCDC** are separately distributed on the acridan donor and DPS acceptor, resulting in a very narrow ΔE_{ST} of 6.2 meV and hole-electron overlap integrals of 0.118 for $S_1 < \Psi_h \Psi_e >$ and 0.116 for $T_1 < \Psi_h \Psi_e >$, respectively. The hole and particle of T_2 mainly distributed on the DPS acceptor and carbazole donor, show a larger ΔE_{TT} of 0.34 eV and a hybrid LE & CT mixed excitation character with a large hole-electron overlap integral ($T_2 < \Psi_h \Psi_e >$) of 0.611. Furthermore, the SOC matrix element (SOCME) value of $\langle S_1|\hat{H}_{SOC}|T_1\rangle$ and $\langle S_1|\hat{H}_{SOC}|T_2\rangle$ is

0.021 and 0.33 cm^{-1}, respectively. However, the higher SOCME value of $\langle S_1|\hat{H}_{SOC}|T_2\rangle$ may not be responsible for a fast RISC process between S_1 and T_2 because the effect of reorganization energies is not negligible. According to the Marcus-Hush theory [17], the rate constants of RISC transition involving the effect of reorganization energy were calculated using the following equation:

$$k_{RISC} = \frac{V^2}{\hbar}\sqrt{\frac{\pi}{k_B T\lambda}}exp\left[-\frac{(\Delta E_{ST}+\lambda)^2}{4k_B T\lambda}\right]$$

where k_{RISC} is the rate constant of RISC, λ is the reorganization energy for the respective transition, ΔE_{ST} is an energy gap between ^{1}CT and the respective triplet state, k_B is the Boltzmann constant, $\hbar$ is the reduced Planck's constant, and T is the temperature (300 K). Due to a very similar geometry and electronic parameters of ^{3}CT and ^{1}CT, the reorganization energy ($\lambda_{1CT\text{-}3CT}$) is only 4.7 meV (Fig. 2**c**). Conversely, the substantial differences in geometries and dipole moments between ^{1}CT and ^{3}LE&^{3}CT states lead to a large reorganization energy ($\lambda_{1CT\text{-}3LE\&3CT}$) of 370.7 meV, which is nearly a hundredfold more than the value of $\lambda_{1CT\text{-}3CT}$. As a result, the calculated k_{RISC} of ^{3}CT → ^{1}CT (1.24×10^6 s^{-1}) is higher than that of ^{3}LE&^{3}CT → ^{1}CT (1.06×10^2 s^{-1}) over 10^4. Thus, the ^{3}LE&^{3}CT → ^{1}CT transition cannot contribute considerably to RISC and the ^{3}CT → ^{1}CT transition can solely afford high RISC rates due to molecular vibrations, even though it is forbidden by the El-Sayed's rules. The SOC value between the ^{3}LE&^{3}CT and ^{1}CT states is ten times higher than the value between the ^{3}CT and ^{1}CT states, but the small $\Delta E_{1CT-\ 3CT}$ energy gap together with comparably a small reorganization energy enable a fast ^{3}CT → ^{1}CT spin-flip rate. The vibrationally assisted RISC model indicates that activated SOC by molecular vibrations plays the key role in facilitating direct RISC with a high rate of ^{3}CT → ^{1}CT transition.

Reorganization energy and Huang-Rhys factor are two effective parameters to measure the nonradiative consumption of excited state energy. The relationship between the reorganization energy between S_1 and T_1 and normal vibration modes is illustrated in **Figure S6**, and we find that the contribution of the low frequency (<200 cm^{-1}) and medium frequency (300–1500 cm^{-1}) and high frequency (>1500 cm^{-1}) modes to the total reorganization energy is significant. These low frequency modes are associated with ring rotations and dihedral angles of molecular fragments, such as the large value of 12.9 cm^{-1} at the 10 cm^{-1} mode for carbazolyl dendrons; the medium frequency mode is assigned to the stretching vibration of C–C and C-S bonds, which bind acceptor to donor units, such as the large value of 35.3 cm^{-1} at the 1144 cm^{-1} mode. The high frequency modes are mainly from C-C and C-N stretching vibrations of acridan donors and dendrons, such as the large value of 12.7 cm^{-1} at the 1689 cm^{-1} mode. Therefore, the reorganization energy between S_1 and T_1 with the synergistic impact of three vibration modes could improve vibrational perturbations and activate the ^{3}CT → ^{1}CT spin-flip process; additionally, the small reorganization energy can also suppress non-radiative energy consumption, which is helpful to enhance the fluorescence efficiency. To further probe the structure–property relationship during the energy conversion processes of $S_1 \leftrightarrow T_1$, we analyzed the Huang-Rhys factors as well as the displacement vectors of vibrational modes with the largest Huang-Rhys factors (**Figure S6**). For the conversion between S_1 and T_1, many low-frequency vibration modes (<100 cm^{-1}) have significant Huang-Rhys factors which correspond to the rotational motion of the dendron carbazolyl groups. This suggests that the free rotation of carbazolyl can provide an important channel to energy conversion between S_1 and T_1. And their large torsional barriers are sure to restrict the nonradiative decay to a large extent owing to significant steric hindrance.

2.3. Photophysical properties

Fig. 3**a,b** show the UV–Vis absorption and fluorescence spectra of **PDCDC**. The polymer exhibits two types of absorption bands: the bands at 250 and 300 nm are mainly attributed to the π-π* transition of carbazole units [48], and the bands at 320–370 nm are mainly attributed to dicarbazole or the electron donor/acceptor units in both compounds [49], which implies stronger charge transfer in films than in solution. The fluorescence spectra of dilute toluene solution and neat film display a similar main emission peak, showing a greenish-blue emission peak at 495 and 496 nm, respectively, with charge transfer characteristics.

Differently, in toluene solution, the polymer shows a blue-shifted fluorescence band assigned to the dicarbazole unit at ~ 380–430 nm. This unit is separated from the TADF segment by the non-conjugated hexyloxy spacer, and the dicarbazole appears not to be involved in intramolecular charge transfer in dilute solution. The fluorescence spectra of pure neat films show a different profile, since for the dicarbazole unit emission is missing at ~ 380–430 nm, indicating stronger overlap between the CT absorption and the blue emission, and shorter distance between donors and acceptors in the film, compared to solution. The phosphorescence spectra of dilute toluene and neat film at 77 K are shown in **Figure S7**. The ΔE_{ST} values are 0.06 in toluene solution and 0.02 eV in films, calculated from the onset energy of the fluorescence and phosphorescence spectra. The small values indicate that the dendronized polymer should readily undergo RISC and be TADF-active. **PDCDC** shows positive solvatochromism of its emission spectra in toluene, chloroform, acetone and dichloromethane (Fig. 3**c**). The Lippert-Mataga plot (ν_{abs}-ν_{em} against polarity of solvent) exhibits a slope of ~ 5120 cm^{-1} for **PDCDC**, indicating that the excited state of the emitter possesses strong charge transfer character [50]. To study the aggregated optical properties, solvent–nonsolvent PL measurements were performed. The very weak emission of **PDCDC** in pure THF solution increases steadily with increasing the content of water and the peak is sharply enhanced at 10:90 (v/v) THF/water mixture, indicating the AEE property of the compound (Fig. 3**d** and **Figure S8**). The enhancement of PL intensity may be caused by the aggregation of the TADF core. The twisted conformation of TADF units will favor loose packing with weak molecular interactions, and thus rotation and vibration will occur easily in the dilute solution. In contrast, in the aggregated state, intramolecular motions are restricted, and thus the nonradiative pathways of the excited state are blocked [44,45]. Therefore, with the increased water fraction, the emission intensities are enhanced.

The electrochemical behavior of the polymer was investigated by cyclic voltammetry (CV) in degassed anhydrous acetonitrile solution (**Figure S9**). The polymer exhibits three quasi-reversible oxidation processes, which can be assigned to the oxidation of DMAC, carbazole dendrons and dicarbazole dendrons, respectively. The HOMO level can be calculated according to the equation $E_{HOMO} = -(E_{(onset,\ ox\ vs\ Fc+/Fc)} + 4.8)$ by CV, and the LUMO level calculated according to the equation LUMO = HOMO + E_g. The values of −5.23 and 1.90 eV for the HOMO and LUMO match well with the data of theoretical simulations.

The ratio between the delayed and prompt fluorescence (DF and PF) was determined from the integration of the steady-state spectra obtained in degassed and aerated conditions; this is because triplets which are involved in DF are quenched by oxygen. The corresponding spectra of **PDCDC** in toluene solutions are shown in Fig. 4**a**. Fig. 4**b** shows the PL lifetime decay curves of the polymer in toluene in the presence and absence of oxygen. These data confirm the TADF performance of the polymer. In the absence of oxygen, **PDCDC** shows double exponential decay curves assigned to the prompt fluorescence in the nanosecond regime and the delayed fluorescence in the microsecond regime. At the same time, **PDCDC** also shows a double exponential decay in the presence of oxygen, which is different from previous DPS-acceptor TADF dendrimers [51]. These data demonstrate that **PDCDC** still exhibits obvious TADF in the presence of oxygen, and this can be explained by shielding of the TADF unit due to the entangled polymer chains. That is, the flexible alkyl linker of **PDCDC** enables the dicarbazole unit to partly shield (encapsulate) the central TADF units and reduce the quenching of the triplet state by oxygen. In addition, the entanglement of polymer chains of **PDCDC** can also restrict the ingress of oxygen into the core of

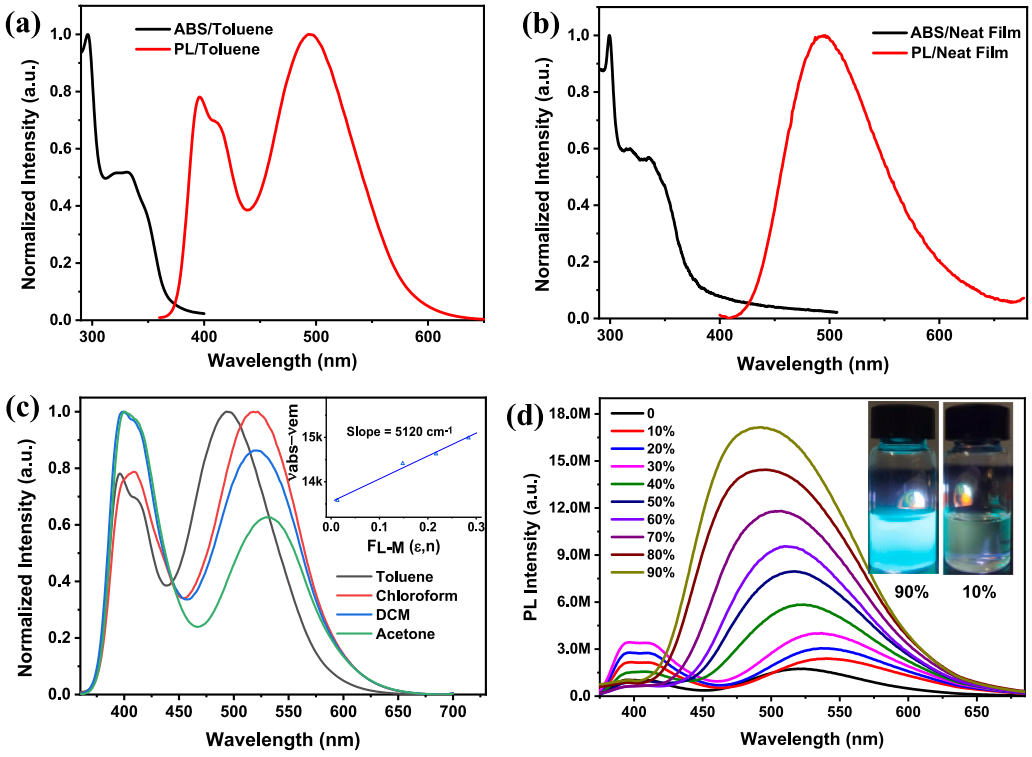

Fig. 3. UV–vis absorption and photoluminescence spectra in toluene solution (a) and neat films (b) of **PDCDC**. Photoluminescence spectra in toluene, chloroform, dichloromethane and acetone solution of **PDCDC** and the corresponding Lippert-Mataga plot (c). PL spectra of **PDCDC** in water/THF mixtures with different fractions of water (d); the inset is fluorescent images of 90% and 10% water/THF solution mixtures under UV light irradiation.

the structure.

The delayed fluorescence lifetimes of **PDCDC** in neat film are 1.95, 1.42 and 1.29 μs at 100, 200 and 300 K, respectively, and the DF ratios are enhanced incrementally from 58.9%, 65.7% to 78.4% with increasing temperatures (Fig. 4**c**). It is notable that the shortest delayed fluorescence lifetime and highest DF ratio are observed at 300 K, suggesting that the higher temperature is more conducive to the effective RISC process. As a comparison, the delayed fluorescence lifetime and ratio is 1.05 μs/68.7% at 300 K in toluene solution. The enhanced delayed fluorescence in the film means loosely packed clusters suppress deformation in large-scale but leave spaces for geometric relaxation that could result in lifetime decay on log scale at a few microseconds. Naturally, the PLQY also increase from 52% in toluene to 68% in neat film, which probably originates from more restricted molecular relaxation and inhomogeneous conformations in condensed states. Indeed, the prompt fluorescence rate (k_{PF}) increases from 5.61 to 6.39 s^{-1}, and the nonradiative decay rate of triplet exciton ($kT\,nr$) decreases from 6.12 to 3.62 s^{-1} when the environment changes from the dilute toluene to the neat film. This behavior can be ascribed to the enhanced cluster aggregation and suppression of the nonradiative deactivation from the flexible molecular skeleton. Moreover, the ISC and RISC rates (k_{ISC} and k_{RISC}) in toluene were calculated to be 2.37×10^7 s^{-1} and 0.77×10^6 s^{-1} while the values were 3.41×10^7 s^{-1} and 1.13×10^6 s^{-1} in the neat film for **PDCDC** (Table 1). Additionally, $K_{ST} = [T_1]/[S_1] = k_{ISC}/k_{RISC}$, which represents the equilibrium population ratio between singlet and triplet states, was calculated using the experimentally determined k_{ISC} and k_{RISC} values. K_{ST} was 30.8 and 30.2 in toluene and the neat film, respectively, indicating that the singlet state is more favorably populated in a solid state. The integral of the delayed fluorescence of the polymer in zeonex, collected with 1 μs delay time and integrated over 100 μs, shows a linear dependence (gradient 1) with excitation power, confirming that DF originates from a monomolecular process – namely TADF (Fig. 4**d**). The possibility of a bimolecular process such as triplet–triplet annihilation (TTA) is excluded by this data [52]. Upon increasing the power to ≥ 10 μJ, the slope decreased to ~ 0.5 indicating the onset of emission quenching (possibly singlet–singlet or triplet–-triplet annihilations) in the polymer.

2.4. OLED performance

Good film-forming ability is one of the most important preconditions for the fabrication of non-doped solution-processed OLEDs. As shown in Fig. 5**a**, the AFM height image displays a homogeneous and integrated surface with small root-mean-square (RMS) roughness values of 0.403 nm for **PDCDC**, suggesting the good film-forming ability. Therefore, the **PDCDC** films are indeed suitable for non-doped light-emitting layers of OLEDs. To investigate electroluminescent (EL) properties of **PDCDC**, non-doped OLEDs were fabricated by solution processing with a configuration of device A: ITO/poly(3,4-ethylenedioxythiophene):poly (styrenesulfonate) (PEDOT:PSS) (40 nm)/ **PDCDC** (EML) (40 nm)/ bis (2(diphenylphosphino)phenyl)ether oxide (DPEPO) (8 nm)/1,3,5-tri(*m*-pyrid-3-yl-phenyl)benzene (TmPyPB) (42 nm)/LiF (1 nm)/Al (100 nm). The device characteristics are shown in Fig. 5**b**, and key performance parameters are listed in Table 2. The devices exhibit sky-blue EL emission with λ_{max} 486 nm ($CIE_{x,y}$: 0.21, 0.35), which is slightly blue shifted compared to its PL spectrum in neat film (Table 1). The device achieves a low turn-on voltage of 3.2 V due to the good matching of energy levels of the component layers. In addition, a maximum EQE of 7.5% and EQE at 100 cd m^{-2} of 7.4% were observed, indicating a very small efficiency roll-off. To further improve the device performance, the device structure was optimized as ITO/ PEDOT:PSS (40 nm)/ poly(*N*-vinylcarbazole) (PVK) (40 nm)/ **PDCDC** (EML) (40 nm)/TmPyPB (42 nm)/LiF (1 nm)/Al (100 nm). In this device B structure, PVK was added as a hole transporting layer, and DPEPO as a hole blocking layer was deleted to favor the hole transport. The optimized device exhibits greenish-blue EL at λ_{max} 498 nm ($CIE_{x,y}$: 0.23, 0.39), which is slightly red-shifted compared

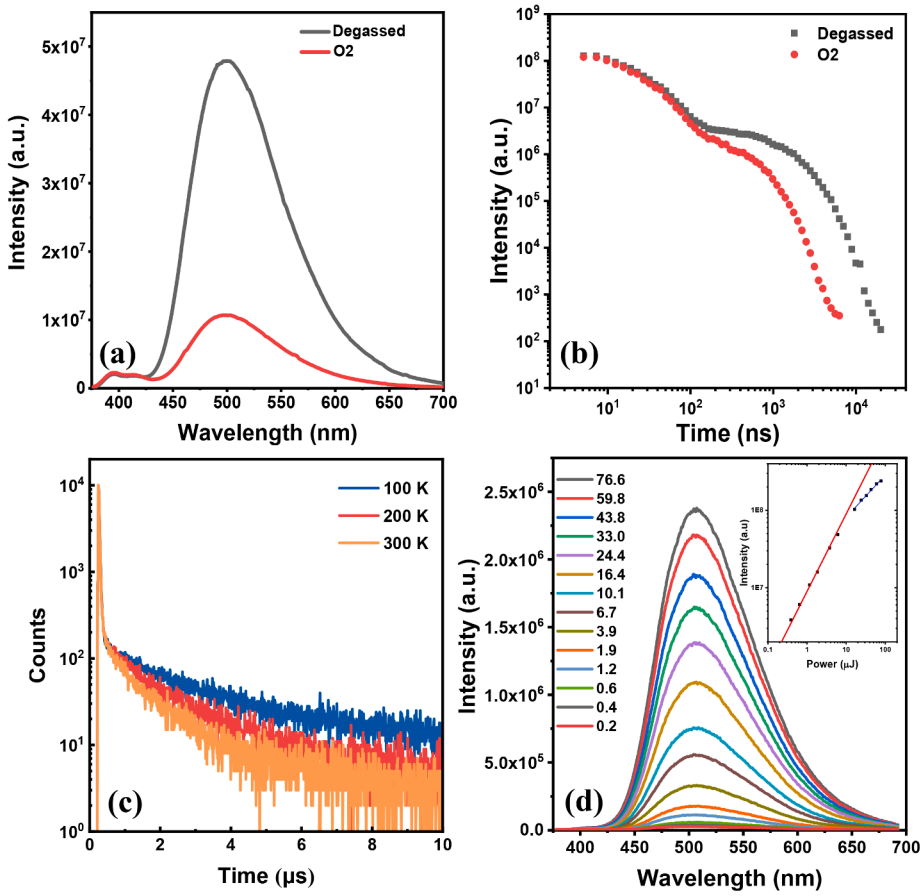

Fig. 4. Photoluminescence spectra (a) and decays (b) in degassed and oxygenated toluene solution of **PDCDC**. Photoluminescence decays in neat films at different temperatures (c). Dependence of DF intensity with excitation power and time resolved PL spectra (d).

Table 1
Photophysical data of **PDCDC.**

	λ_{PL}[a] (nm)	τ_{PF}/R_{PF}[b] (ns/%)	τ_{DF}/R_{DF}[c] (μs/%)	S_1/T_1[d] (eV)	ΔE_{ST}[e] (eV)	Φ_{PL}[f] (%)	k_{PF}[g] (10^6 s^{-1})	$kT\,nr$[h] (10^5 s^{-1})	k_{ISC}[i] (10^7 s^{-1})	k_{RISC}[j] (10^6 s^{-1})
Toluene solution	495	29/31.3	1.05/68.7	2.99/2.93	0.06	52	5.61	6.12	2.37	0.77
Neat films	496	23/21.6	1.29/78.4	2.88/2.86	0.02	68	6.39	3.62	3.41	1.13

[a] Maximum photoluminescence peak. [b]Prompt fluorescence lifetime and ratio. [c]Delayed fluorescence lifetime and ratio. [l]Lowest singlet and triplet states energy level. [e]$\Delta E_{ST} = S_1 - T_1$. [f]Absolute PL quantum yield determined by a calibrated integrating sphere in air; error ± 1%. [g]The rate constant of prompt fluorescence from $k_{PF} = \Phi_{PF}/\tau_{PF}$ and $\Phi_{PF} = \Phi_{PL}{}^*R_{PF}$. [h]The nonradiative decay rate of triplet exciton calculated from $k_{nr}^T = \frac{1-\Phi_{DF}}{\tau_{DF}}$ and $\Phi_{DF} = \Phi_{PL}{}^*R_{DF}$. [i] The intersystem crossing rates from $k_{ISC} = \frac{\Phi_{DF}}{\tau_{PF} \times (\Phi_{PF} + \Phi_{DF})}$. [j] The reverse intersystem crossing rates from $k_{RISC} = \frac{\Phi_{PL}}{\tau_{DF} \times (1 - \Phi_{DF})}$.

to Device A and is almost identical to the PL spectrum of **PDCDC** in neat film. Device B achieves a maximum luminance of 498 cd m^{-2}, a maximum current efficiency (CE) of 23.1 cd A^{-1}, and a maximum power efficiency (PE) of 16.5 lm W^{-1}. Although the turn-on voltage was slightly increased to 3.6 V, a higher maximum EQE of 9.0% was observed, which is the highest efficiency for blue and greenish-blue dendronized polymer OLEDs (Fig. 5**c**). The device can achieve this performance not only due to its balanced hole/electron-transporting abilities (**Figure S10**) but also owing to the good film-forming ability. The lower turn-on voltage of device A could improve exciton diffusion distance and broaden the exciton recombination region, which favours lower efficiency roll-off. The EQE and luminance of the devices are probably limited by aggregation and exciton concentration quenching due to the close proximity of the luminescent units, as generally observed in homopolymers.[30] Indeed, higher efficiency devices (EQE_{max} 24%) were obtained using the (non-polymerized) pendant monomer unit as the emitter [61].

3. Conclusions

In summary, a new kind of TADF polymer was designed and synthesized via the conjugated and non-conjugated linkages of carbazoles. A half-dendronized TADF core and a half-encapsulated dicarbazole unit were integrated, and then the linear dendronized polymer **PDCDC** was obtained by introducing the main alkyl polymer chain as the backbone. The theoretical simulations show that ^{1}CT ↔ ^{3}CT transitions could be effectively activated due a combination of the vibrationally enhanced SOC, very small energy gap, and comparably small reorganization energy originating from similar geometries in the ^{1}CT and ^{3}CT states. In contrast, a much larger reorganization energy $\lambda_{1CT-3LE\&3CT}$ value and decreasing population of the ^{3}LE&^{3}CT state result in negligible contribution of ^{3}LE&^{3}CT ↔ ^{1}CT transition rate. The dendronized polymer displays excellent TADF properties due to not only the conjugated and non-conjugated dendrons minimizing the fluorescence concentration quenching, but also the entangled polymeric backbone which inhibits

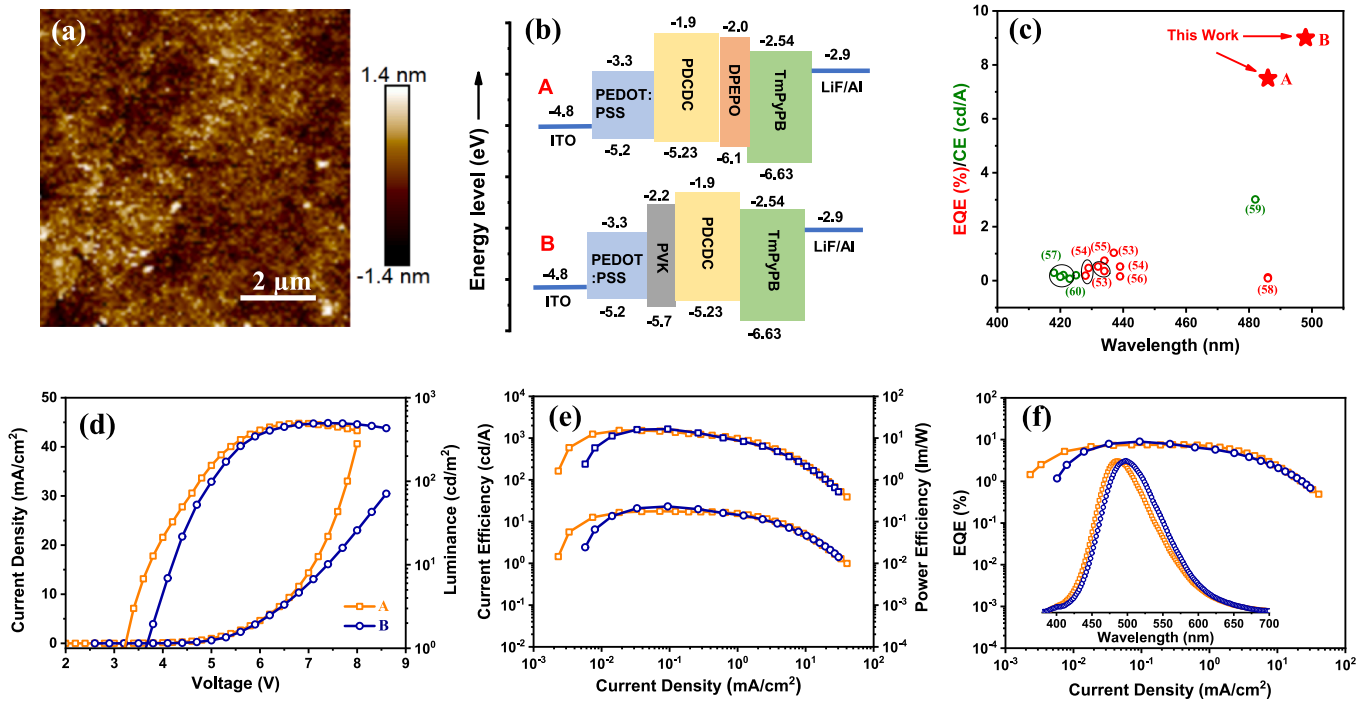

Fig. 5. (a) AFM topographic images of the solution-processed neat films for **PDCDC**. (b) Energy-level diagrams and structures of OLED devices A and B. (c) EL efficiency data based on blue and greenish-blue dendronized polymers (red dots for EQE and green dots for CE) [53–60] (d) Current density–voltage-luminance curves. (e) Current efficiency- current density-power efficiency curves. (f) External quantum efficiency versus current density curves of the devices. The inset is normalized EL spectra at 5 V. (For interpretation of the references to colour in this figure legend, the reader is referred to the web version of this article.)

Table 2
Performance data of **PDCDC** based OLEDs.

devices	V_{on}[a] (V)	CE_{max}[b] (cd/A)	PE_{max}[c] (lm/W)	EQE_{max}[d] (%)	EQE_{100}[e] (%)	λ_{EL}[f] (nm)	CIE[f] (x,y)
A	3.2	17.7	15.2	7.5	7.4	486	(0.21, 0.35)
B	3.6	23.1	16.5	9.0	6.5	498	(0.23, 0.39)

[a] The voltage at 1 cd/m^2. [b]Maximum current efficiency. [c]Maximum power efficiency. [d]Maximum external quantum efficiency. [e]External quantum efficiency at 100 cd m^{-2}. [f]EL emission peak and CIE coordinates at 5 V.

the ingress of oxygen. Besides, the polymer exhibits obvious AEE property, minimizing the exciton quenching in aggregated states, and consequently increases EL efficiency in devices. An EQE_{max} of 9.0% for host-free **PDCDC**-based devices has been obtained, which is the highest reported value for blue and greenish-blue dendronized polymer OLEDs. These results present a new direction for the study of TADF macromolecules and their highly efficient undoped solution-processable devices.

Declaration of Competing Interest

The authors declare that they have no known competing financial interests or personal relationships that could have appeared to influence the work reported in this paper.

Acknowledgements

Zhongjie Ren acknowledges NSFC (No. 51922021) for funding. Yuchao Liu acknowledges NSFC (No. 52103220) for funding. Shouke Yan acknowledges Shandong Provincial Natural Science Foundation (ZR2019ZD50) for funding. F. B. D. and M. R. B. acknowledge the EPSRC for funding under grant numbers EP/L02621X/1 and EP/N028511/1.

Appendix A. Supplementary data

Supplementary data to this article can be found online at https://doi.org/10.1016/j.cej.2022.134924.

References

[1] C.A. Parker, C.G. Hatchard, Triplet-singlet emission in fluid solutions. phosphorescence of eosin, Trans. Faraday Soc. 57 (1961) 1894–1904. https://pubs.rsc.org/en/content/articlepdf/1961/tf/tf9615701894.
[2] H. Uoyama, K. Goushi, K. Shizu, H. Nomura, C. Adachi, Highly efficient organic light-emitting diodes from delayed fluorescence, Nature 492 (7428) (2012) 234–238, https://doi.org/10.1038/nature11687.
[3] C. Adachi, Third-generation organic electroluminescence materials, Jpn J. Appl. Phys. 53 (6) (2014) 060101, https://doi.org/10.7567/JJAP.53.060101.
[4] F.B. Dias, K.N. Bourdakos, V. Jankus, K.C. Moss, K.T. Kamtekar, V. Bhalla, J. Santos, M.R. Bryce, A.P. Monkman, Triplet harvesting with 100% efficiency by way of thermally activated delayed fluorescence in charge transfer OLED emitters, Adv. Mater. 25 (27) (2013) 3707–3714, https://doi.org/10.1002/adma.201300753.
[5] M.Y. Wong, E. Zysman-Colman, Purely organic thermally activated delayed fluorescence materials for organic light-emitting diodes, Adv. Mater. 29 (22) (2017) 1605444, https://doi.org/10.1002/adma.201605444.
[6] L. Yu, Z. Wu, G. Xie, C. Zhong, Z. Zhu, H. Cong, D. Ma, C. Yang, Achieving a balance between small singlet-triplet energy splitting and high fluorescence radiative rate in a quinoxaline-based orange-red thermally activated delayed fluorescence emitter, Chem. Commun. 52 (73) (2016) 11012–11015, https://doi.org/10.1039/C6CC05203G.
[7] D.S.M. Ravinson, M.E. Thompson, Thermally assisted delayed fluorescence (TADF): fluorescence delayed is fluorescence denied, Mater. Horiz. 7 (5) (2020) 1210–1217, https://doi.org/10.1039/d0mh00276c.
[8] H. Noda, X.-K. Chen, H. Nakanotani, T. Hosokai, M. Miyajima, N. Notsuka, Y. Kashima, J.-L. Brédas, C. Adachi, Critical role of intermediate electronic states for spin-flip processes in charge-transfer-type organic molecules with multiple donors and acceptors, Nat. Mater. 18 (10) (2019) 1084–1090, https://doi.org/10.1038/s41563-019-0465-6.
[9] T. Serevičius, R. Skaisgiris, I. Fiodorova, G. Kreiza, D. Banevičius, K. Kazlauskas, S. Tumkevičius, S. Juršėnas, Single-exponential solid-state delayed fluorescence decay in TADF compounds with minimized conformational disorder, J. Mater. Chem. C 9 (3) (2021) 836–841, https://doi.org/10.1039/d0tc05503d.

[10] P.K. Samanta, D. Kim, V. Coropceanu, J.-L. Brédas, Up-Conversion Intersystem Crossing Rates in Organic Emitters for Thermally Activated Delayed Fluorescence: Impact of the Nature of Singlet vs Triplet Excited States, J. Am. Chem. Soc. 139 (11) (2017) 4042–4051, https://doi.org/10.1021/jacs.6b1212410.1021/jacs.6b12124.s001.
[11] T. Ogiwara, Y. Wakikawa, T. Ikoma, Mechanism of intersystem crossing of thermally activated delayed fluorescence molecules, J. Phys. Chem. A 119 (14) (2015) 3415–3418, https://doi.org/10.1021/acs.jpca.5b02253.
[12] M. K. Etherington, J. Gibson, H. F. Higginbotham, T. J. Penfold, A. P. Monkman, Revealing the spin-vibronic coupling mechanism of thermally activated delayed fluorescence, Nat. Commun. 7 (2016) 13680. https://doi.org/ 10.1038/ncomms13680.
[13] J. Feng, A.-P. Reponen, A.S. Romanov, M. Linnolahti, M. Bochmann, N. C. Greenham, T. Penfold, D. Credgington, Influence of Heavy Atom Effect on the Photophysics of Coinage Metal Carbene-Metal-Amide Emitters, Adv. Funct. Mater. 31 (1) (2021) 2005438, https://doi.org/10.1002/adfm.202005438.
[14] E. Laborda, M.C. Henstridge, C. Batchelor-McAuley, R.G. Compton, Asymmetric Marcus-Hush theory for voltammetry, Chem. Soc. Rev. 42 (12) (2013) 4894–4905, https://doi.org/10.1039/c3cs35487c.
[15] H. Yersin, L. Mataranga-Popa, R. Czerwieniec, Y. Dovbii, Design of a New Mechanism beyond Thermally Activated Delayed Fluorescence toward Fourth Generation Organic Light Emitting Diodes, Chem. Mater. 31 (16) (2019) 6110–6116, https://doi.org/10.1021/acs.chemmater.9b0116810.1021/acs.chemmater.9b01168.s001.
[16] F. Dinkelbach, M. Bracker, M. Kleinschmidt, C.M. Marian, Large Inverted Singlet-Triplet Energy Gaps Are Not Always Favorable for Triplet Harvesting: Vibronic Coupling Drives the (Reverse) Intersystem Crossing in Heptazine Derivatives, J. Phys. Chem. A 125 (46) (2021) 10044–10051, https://doi.org/10.1021/acs.jpca.1c0915010.1021/acs.jpca.1c09150.s001.
[17] I.E. Serdiuk, M. Mońka, K. Kozakiewicz, B. Liberek, P. Bojarski, S.Y. Park, Vibrationally Assisted Direct Intersystem Crossing between the Same Charge-Transfer States for Thermally Activated Delayed Fluorescence: Analysis by Marcus-Hush Theory Including Reorganization Energy, J. Phys. Chem. B 125 (10) (2021) 2696–2706, https://doi.org/10.1021/acs.jpcb.0c1060510.1021/acs.jpcb.0c10605.s001.
[18] X.K. Chen, D. Kim, J.L. Bredas, Thermally Activated Delayed Fluorescence (TADF) Path toward Efficient Electroluminescence in Purely Organic Materials: Molecular Level Insight, Acc. Chem. Res. 51 (9) (2018) 2215–2224, https://doi.org/10.1021/acs.accounts.8b00174.
[19] Y. Liu, C. Li, Z. Ren, S. Yan, M.R. Bryce, All-organic thermally activated delayed fluorescence materials for organic light-emitting diodes, Nat. Rev. Mater. 3 (2018) 18020, https://doi.org/10.1038/natrevmats.2018.20.
[20] S. Ho, S. Liu, Y. Chen, F. So, Review of recent progress in multilayer solution-processed organic light-emitting diodes, J. Photonics Energy 5 (1) (2015) 057611, https://doi.org/10.1117/1.JPE.5.057611.
[21] Q. Wei, Z. Ge, B. Voit, Thermally activated delayed fluorescent polymers: structures, properties, and applications in OLED devices, Macromol. Rapid Commun. 40 (1) (2018) 1800570, https://doi.org/10.1002/marc.201800570.
[22] Y. Zou, S. Gong, G. Xie, C. Yang, Design strategy for solution-processable thermally activated delayed fluorescence emitters and their applications in organic light-emitting diodes, Adv. Opt. Mater. 6 (23) (2018) 1800568, https://doi.org/10.1002/adom.201800568.
[23] R.S. Nobuyasu, Z. Ren, G.C. Griffiths, A.S. Batsanov, P. Data, S. Yan, A. P. Monkman, M.R. Bryce, F.B. Dias, Rational Design of TADF Polymers Using a Donor-Acceptor Monomer with Enhanced TADF Efficiency Induced by the Energy Alignment of Charge Transfer and Local Triplet Excited States, Adv. Opt. Mater. 4 (4) (2016) 597–607, https://doi.org/10.1002/adom.201500689.
[24] S.Y. Lee, T. Yasuda, H. Komiyama, J. Lee, C. Adachi, Thermally Activated Delayed Fluorescence Polymers for Efficient Solution-Processed Organic Light-Emitting Diodes, Adv. Mater. 28 (21) (2016) 4019–4024, https://doi.org/10.1002/adma.201505026.
[25] C. Li, Z. Ren, X. Sun, H. Li, S. Yan, Deep-Blue Thermally Activated Delayed Fluorescence Polymers for Nondoped Solution-Processed Organic Light-Emitting Diodes, Macromolecules 52 (6) (2019) 2296–2303, https://doi.org/10.1021/acs.macromol.9b00083.
[26] X. Zeng, J. Luo, T. Zhou, T. Chen, X. Zhou, K. Wu, Y. Zou, G. Xie, S. Gong, C. Yang, Using Ring-Opening Metathesis Polymerization of Norbornene To Construct Thermally Activated Delayed Fluorescence Polymers: High-Efficiency Blue Polymer Light-Emitting Diodes, Macromolecules 51 (5) (2018) 1598–1604, https://doi.org/10.1021/acs.macromol.7b02629.
[27] S. Shao, J. Hu, X. Wang, L. Wang, X. Jing, F. Wang, Blue Thermally Activated Delayed Fluorescence Polymers with Nonconjugated Backbone and Through-Space Charge Transfer Effect, J. Am. Chem. Soc. 139 (49) (2017) 17739–17742, https://doi.org/10.1021/jacs.7b1025710.1021/jacs.7b10257.s001.
[28] Q. Li, J. Hu, J. Lv, X. Wang, S. Shao, L. Wang, X. Jing, F. Wang, Through-Space Charge-Transfer Polynorbornenes with Fixed and Controllable Spatial Alignment of Donor and Acceptor for High-Efficiency Blue Thermally Activated Delayed Fluorescence, Angew. Chem. Int. Ed. 59 (45) (2020) 20174–20182, https://doi.org/10.1002/anie.202008912.
[29] X. He, D. Cai, D.-Y. Kang, W. Haske, Y. Zhang, C.A. Zuniga, B.H. Wunsch, S. Barlow, J. Leisen, D. Bucknall, B. Kippelen, S.R. Marder, Phosphorescent light-emitting diodes using triscarbazole/bis(oxadiazole) hosts: comparison of homopolymer blends and random and block copolymers, J. Mater. Chem. C 2 (33) (2014) 6743–6751, https://doi.org/10.1039/C4TC01079E.
[30] Z. Ren, R.S. Nobuyasu, F.B. Dias, A.P. Monkman, S. Yan, M.R. Bryce, Pendant Homopolymer and Copolymers as Solution-Processable Thermally Activated Delayed Fluorescence Materials for Organic Light-Emitting Diodes, Macromolecules 49 (15) (2016) 5452–5460, https://doi.org/10.1021/acs.macromol.6b0121610.1021/acs.macromol.6b01216.s001.
[31] S.H. Hwang, C.N. Moorefield, G.R. Newkome, Dendritic macromolecules for organic light-emitting diodes, Chem. Soc. Rev. 37 (11) (2008) 2543–2557, https://doi.org/10.1039/B803932C.
[32] K. Albrecht, K. Matsuoka, K. Fujita, K. Yamamoto, Carbazole dendrimers as solution-processable thermally activated delayed-fluorescence materials, Angew. Chem. Int. Ed. 54 (19) (2015) 5677–5682, https://doi.org/10.1002/anie.201500203.
[33] A. Zhang, L. Shu, Z. Bo, A.D. Schlüter, Dendronized Polymers: Recent Progress in Synthesis, Macromol. Chem. Phys. 204 (2) (2003) 328–339, https://doi.org/10.1002/macp.200290086.
[34] H. Frauenrath, Dendronized polymers-building a new bridge from molecules to nanoscopic objects, Prog. Polym. Sci. 30 (3–4) (2005) 325–384, https://doi.org/10.1016/j.progpolymsci.2005.01.011.
[35] X. Liu, W. Lin, D. Astruc, H. Gu, Syntheses and applications of dendronized polymers, Prog. Polym. Sci. 96 (2019) 43–105, https://doi.org/10.1016/j.progpolymsci.2019.06.002.
[36] J.W. Levell, J.P. Gunning, P.L. Burn, J. Robertson, I.D.W. Samuel, A phosphorescent poly(dendrimer) with increased viscosity for solution-processed OLED devices, Org. Electron. 11 (9) (2010) 1561–1568, https://doi.org/10.1016/j.orgel.2010.05.011.
[37] J.P. Gunning, J.W. Levell, M.F. Wyatt, P.L. Burn, J. Robertson, I.D.W. Samuel, The development of poly(dendrimer)s for advanced processing, Polym. Chem. 1 (5) (2010) 730–738, https://doi.org/10.1039/C0PY00039F.
[38] W.-Y. Lai, J.W. Levell, A.C. Jackson, S.-C. Lo, P.V. Bernhardt, I.D.W. Samuel, P. L. Burn, A Phosphorescent Poly(dendrimer) Containing Iridium(III) Complexes: Synthesis and Light-Emitting Properties, Macromolecules 43 (17) (2010) 6986–6994, https://doi.org/10.1021/ma101363h.
[39] J.W. Levell, S. Zhang, W.-Y. Lai, S.-C. Lo, P.L. Burn, I.D.W. Samuel, High Power Efficiency Phosphorescent Poly(dendrimer) OLEDs, Opt. Express 20 (S2) (2012) A213–A218, https://doi.org/10.1364/OE.20.00A213.
[40] S.M. Russell, J. Jang, A.M. Brewer, D.M. Stoltzfus, E.V. Puttock, P.L. Burn, A red emissive poly(dendrimer) for solution processed organic light-emitting diodes, Org. Electron. 78 (2020) 105594, https://doi.org/10.1016/j.orgel.2019.105594.
[41] F. Maasoumi, R.D. Jansen-van Vuuren, P.E. Shaw, E.V. Puttock, R.C.R. Nagiri, J. A. McEwan, M. Bown, J.L. O'Connell, C.J. Dunn, P.L. Burn, E.B. Namdas, An external quantum efficiency of >20% from solution-processed poly(dendrimer) organic light-emitting diodes, npj Flexible Electron. 2 (1) (2018) 27, https://doi.org/10.1038/s41528-018-0038-9.
[42] C.Y. Chan, M. Tanaka, H. Nakanotani, C. Adachi, Efficient and stable sky-blue delayed fluorescence organic light-emitting diodes with CIEy below 0.4, Nat. Commun. 9 (1) (2018) 5036, https://doi.org/10.1038/s41467018-07482-6.
[43] C. Li, R.S. Nobuyasu, Y. Wang, F.B. Dias, Z. Ren, M.R. Bryce, S. Yan, Solution-Processable Thermally Activated Delayed Fluorescence White OLEDs Based on Dual-Emission Polymers with Tunable Emission Colors and Aggregation Enhanced Emission Properties, Adv. Opt. Mater. 5 (20) (2017) 1700435, https://doi.org/10.1002/adom.201700435.
[44] L. Tu, Y. Xie, Z. Li, B. Tang, Aggregation-induced emission: Red and near-infrared organic light-emitting diodes, SmartMat 2 (3) (2021) 326–346, https://doi.org/10.1002/smm2.1060.
[45] Y. Wang, J. Yang, Y. Gong, M. Fang, Z. Li, B.Z. Tang, Host–guest materials with room temperature phosphorescence: Tunable emission color and thermal printing patterns, SmartMat 1(1) (2020) e1006. https://doi.org/ 10.1002/smm2.1006.
[46] W. Song, I. Lee, J.Y. Lee, Host Engineering for High Quantum Efficiency Blue and White Fluorescent Organic Light-Emitting Diodes, Adv. Mater. 27 (29) (2015) 4358–4363, https://doi.org/10.1002/adma.201501019.
[47] T. Lu, F. Chen, Multiwfn: a multifunctional wavefunction analyzer, J. Comput. Chem. 33 (5) (2012) 580–592, https://doi.org/10.1002/jcc.22885.
[48] M. Gantenbein, M. Hellstern, L. Le Pleux, M. Neuburger, M. Mayor, New 4,4′-Bis(9-carbazolyl)–Biphenyl Derivatives with Locked Carbazole-Biphenyl Junctions: High-Triplet State Energy Materials, Chem. Mater. 27 (5) (2015) 1772–1779, https://doi.org/10.1021/cm5045754.
[49] K. Albrecht, K. Yamamoto, Dendritic Structure Having a Potential Gradient: New Synthesis and Properties of Carbazole Dendrimers, J. Am. Chem. Soc. 131 (6) (2009) 2244–2251, https://doi.org/10.1021/ja807312e.
[50] W. Li, D. Liu, F. Shen, D. Ma, Z. Wang, T. Feng, Y. Xu, B. Yang, Y. Ma, A Twisting Donor-Acceptor Molecule with an Intercrossed Excited State for Highly Efficient, Deep-Blue Electroluminescence, Adv. Funct. Mater. 22 (13) (2012) 2797–2803, https://doi.org/10.1002/adfm.201200116.
[51] J. Luo, S. Gong, Y. Gu, T. Chen, Y. Li, C. Zhong, G. Xie, C. Yang, Multi-carbazole encapsulation as a simple strategy for the construction of solution-processed, non-doped thermally activated delayed fluorescence emitters, J. Mater. Chem. C 4 (13) (2016) 2442–2446, https://doi.org/10.1039/C6TC00418K.
[52] F.B. Dias, Kinetics of thermal-assisted delayed fluorescence in blue organic emitters with large singlet-triplet energy gap, Philos. Trans. A Math. Phys. Eng. Sci. 373 (2044) (2015) 20140447, https://doi.org/10.1098/rsta.2014.0447.
[53] Q. Peng, J. Xu, M. Li, W. Zheng, Blue Emitting Polyfluorenes Containing Dendronized Carbazole and Oxadiazole Pendants: Synthesis, Optical Properties, and Electroluminescent Properties, Macromolecules 42 (15) (2009) 5478–5485, https://doi.org/10.1021/ma9008737.
[54] H. Jin, W. Zhang, D. Wang, Z. Chu, Z. Shen, D. Zou, X. Fan, Q. Zhou, Dendron-Jacketed Electrophosphorescent Copolymers: Improved Efficiency and Tunable Emission Color by Partial Energy Transfer, Macromolecules 44 (24) (2011) 9556–9564, https://doi.org/10.1021/ma2018556.

[55] H. Jin, Y. Xu, Z. Shen, D. Zou, D. Wang, W. Zhang, X. Fan, Q. Zhou, Jacketed Polymers with Dendritic Carbazole Side Groups and Their Applications in Blue Light-Emitting Diodes, Macromolecules 43 (20) (2010) 8468–8478, https://doi.org/10.1021/ma101814m.
[56] W. Zhang, H. Jin, F. Zhou, Z. Shen, D. Zou, X. Fan, Synthesis and characterization of electrophosphorescent jacketed conjugated polymers, J. Polym. Sci. A Polym. Chem. 50 (18) (2012) 3895–3903, https://doi.org/10.1002/pola.26189.
[57] W. Zhang, H. Jin, D. Wang, Z. Chu, Z. Shen, D. Zou, X. Fan, Jacketed homopolymer with bipolar dendritic side groups and its applications in electroluminescent devices, J. Polym. Sci. A Polym. Chem. 50 (3) (2012) 581–589, https://doi.org/10.1002/pola.25067.
[58] Ş.C. Cevher, D. Keles, G. Hizalan, L. Toppare, A. Cirpan, Alkyl-end phenanthroimidazole modification of benzotriazole based conjugated polymers for optoelectronic applications, Synth. Met. 244 (2018) 1–9, https://doi.org/10.1016/j.synthmet.2018.06.007.
[59] S. Setayesh, A.C. Grimsdale, T. Weil, V. Enkelmann, K. Müllen, F. Meghdadi, E.J. W. List, G. Leising, Polyfluorenes with Polyphenylene Dendron Side Chains: Toward Non-Aggregating, Light-Emitting Polymers, J. Am. Chem. Soc. 123 (5) (2001) 946–953, https://doi.org/10.1021/ja0031220.
[60] A. Pogantsch, F.P. Wenzl, E.J.W. List, G. Leising, A.C. Grimsdale, K. Müllen, Polyfluorenes with Dendron Side Chains as the Active Materials for Polymer Light-Emitting Devices, Adv. Mater. 14 (15) (2002) 1061–1064, https://doi.org/10.1002/1521-4095(20020805)14:15<1061::AID-ADMA1061>3.0.CO;2-6.
[61] C. Li, A. K. Harrison, Y. Liu, Z. Zhao, C. Zeng, F. B. Dias, Z. Ren, S. Yan, M. R. Bryce, Asymmetrical-Dendronized TADF Emitters for Efficient Non-doped Solution-Processed OLEDs by Eliminating Degenerate Excited States and Creating Solely Thermal Equilibrium Routes, Angew. Chem. Int. Ed. 10.1002/anie.202115140.